

Solvent Structure, Dynamics, and Ion Mobility in Aqueous Solutions at 25 °C

S. Koneshan,[†] Jayendran C. Rasaiah,^{*,†} R. M. Lynden-Bell,[‡] and S. H. Lee[§]*Department of Chemistry, University of Maine, Orono, Maine 04469 Atomistic Simulation Group, School of Mathematics and Physics, The Queen's University, Belfast BT7 INN, U.K. Department of Chemistry, Kyungshung University, Pusan 608-736, Korea**Received: January 6, 1998; In Final Form: March 13, 1998*

We calculate the mobilities u_i of the metal cations Li^+ , Na^+ , K^+ , Rb^+ , Cs^+ , and Ca^{2+} and the halides F^- , Cl^- , Br^- , and I^- at infinite dilution by molecular dynamics simulation using the SPC/E model for water at 25 °C and a reaction field for the long-range interactions. The ion mobilities show the same trends as the experimental results with distinct maxima for cations and anions. The mobilities (defined by $u_i = D_i/kT$) of the corresponding uncharged species are also determined by simulation and are in qualitative agreement with Stokes' law. The mobilities of Li^+ , Na^+ , K^+ , Rb^+ and F^- increase on discharge, whereas Cl^- , Br^- , and I^- have smaller mobilities than the corresponding anions. The mobility of the fictitious I^+ ion, which differs from I^- only in its charge, lies between that of I^- and I in the order $u_{\text{I}^-} < u_{\text{I}^+} < u_{\text{I}}$. The residence time of water in the first solvation shell of small cations (Li^+ and Na^+) and Ca^{2+} decreases when the ions are discharged, while the opposite is observed on neutralizing I^- , suggesting the formation of a solvent cage around the large uncharged I which partially breaks up on charging, increasing the mobility of the corresponding ion. The cage breakup is greater for I^- than for I^+ which correlates with the asymmetry in the entropies of solvation of I^- and I^+ , in SPC/E water on charge reversal, providing an explanation for the trends in the mobilities of I , I^- , and I^+ . The residence times of water in the primary hydration shell around cations pass through a minimum as a function of size that correlates with the maximum in the corresponding solvation entropy, suggesting different types of hydration, i.e., electrostatic ion solvation (hydrophilic) and cage formation (hydrophobic) respectively for small and large cations. The results are in accord with recent calculations of the solvation entropy and free energy as continuous functions of the charge and size (Lynden-Bell, R. M.; Rasaiah, J. C. *J. Chem. Phys.* **1997**, *107*, 1981). Hydrophilic and hydrophobic solvation are reflected in the exchange dynamics of the water in the hydration shells around charged and uncharged solutes. The solvation dynamics of individual cations and anions are distinct at short times but characterized by the solvent at long times. Solvent dynamics, structure, and caging modulated by the charge and size of the ions are strongly implicated in determining their mobilities.

I. Introduction

The variation in the mobility of ions in solution as a function of concentration has been studied experimentally for many years and theories due to Debye and Falkenhagen,¹ Fuoss and Onsager,² Friedman,³ and Justice⁴ explain the concentration dependence in dilute solutions. However, the mobility at infinite dilution, where interionic interactions are absent, is still not fully understood in relation to the size and charge of the ions and its dependence on the equilibrium and dynamical properties of the solvent. Water is also an exceptional solvent due to hydrogen bonding and network structure, and its dynamics and structure are perturbed by an ion. This is reflected in an ion's mobility and leads to unusual behavior in aqueous solutions that we study by computer simulation of model systems.

A fundamental problem that requires a detailed explanation is the observed maximum in the mobilities of the ions in aqueous solution at infinite dilution as a function of size and its weaker dependence on the sign of the ion charge; see Figure 1. The latter observation immediately rules out simple molecular (e.g., dipolar solvent) or dielectric continuum models of the solvent

that respond identically or symmetrically to positive and negative ions of the same charge magnitude and size. A second problem is to understand the influence of solvent dynamics and structure on ion mobility at infinite dilution.

The mobility u_i of an ion is its drift velocity divided by the external electric field. It is directly proportional to the charge q_i and inversely proportional to the friction ζ_i so that $u_i = q_i/\zeta_i$. Theories of ion mobilities at infinite dilution were originally developed using continuum models by Max Born,⁵ Fuoss,⁶ Boyd,⁷ Zwanzig,⁸ Hubbard, Onsager, and Kayser,⁹ and Chen and Adelman.¹⁰ They provided the conceptual basis for discussions of ion mobility through their recognition of dielectric ζ_i^{D} and hydrodynamic friction ζ_i^{H} as the primary forces retarding the motion of an ion in a solvent. The total friction, decomposed into these components is

$$\zeta_i = \zeta_i^{\text{H}} + \zeta_i^{\text{D}} \quad (1.1)$$

The hydrodynamic friction is proportional to the ion size and is given by Stokes law. With slip boundary conditions

$$\zeta_i^{\text{H}} = 4\pi\eta R_i \quad (1.2)$$

where R_i is the radius and η is the solvent viscosity. In continuum treatments, the dynamical properties of the solvent

* Corresponding author; rasaiah@maine.maine.edu.

† University of Maine.

‡ The Queen's University.

§ Kyungshung University.

are usually characterized by a single relaxation time τ_D and the dielectric friction varies inversely as some power of the radius R_i . This reduces the mobility when R_i is small and explains qualitatively the maximum in the mobility as a function of the size. In Zwanzig's theory for example,

$$\zeta_i^D = 3q_i^2(\epsilon_o - \epsilon_\infty)\tau_D/(4R_i^3\epsilon_o^2) \quad (1.3)$$

where ϵ_o and ϵ_∞ are the static and high-frequency dielectric constants of the solvent. It is symmetric with respect to the charge and comparatively short-ranged through its variation inversely with the cube of the ion radius. Hubbard and Onsager (HO) developed a more complete formulation at the continuum level which leads to a smaller dielectric friction than that predicted by Zwanzig. Neither of these continuum theories differentiates between positive and negative ions of the same size but agreement with experimental results can be obtained for ions of one charge type (e.g., anions) by treating the viscosity as an adjustable parameter.¹¹ Chen and Adelman¹⁰ extended the continuum model to include the effects of local solvent structure and dynamics.

In molecular theories,^{12,13} the friction coefficient ζ in the Brownian limit is calculated from

$$\zeta_i = 1/(3kT) \int_0^\infty \langle \mathbf{F}_i(t) \mathbf{F}_i(0) \rangle dt \quad (1.4)$$

where $\mathbf{F}_i(t)$ is the random force on a stationary ion at time t and $\langle \mathbf{F}_i(t) \mathbf{F}_i(0) \rangle$ is the equilibrium random force autocorrelation function on this ion. Wolynes¹² developed this by splitting the random force autocorrelation function into components arising from the correlations between the hard repulsive (H) and soft attractive (S) contributions to the force, so that $\zeta_i = \zeta_i^{HH} + \zeta_i^{SH} + \zeta_i^{HS} + \zeta_i^{SS}$ where the hard self-correlation ζ_i^{HH} is identified with the hydrodynamic drag ζ_i^H associated with Stokes' law. Thus, instead of two components there are four, but Wolynes ignores the correlations between the soft and hard components (ζ_i^{SH} and ζ_i^{HS}) because they relax on different time scales and focuses on the time dependence of the fluctuations of the soft forces, i.e., ζ_i^{SS} . These fluctuations, when analyzed approximately, provide an expression for the dielectric drag and the total friction

$$\zeta_i = \zeta_i^{HH} + (1/3kT)\langle F_s^2 \rangle \tau_F \quad (1.5)$$

where $\langle F_s^2 \rangle$ is the static mean square fluctuation in the soft forces and τ_F is their characteristic decay time. The theory incorporates the "solventberg" picture and the continuum dielectric friction model as limiting cases. The molecular theory has been generalized and extended recently by Biswas and Bagchi.¹³ They also ignore the cross terms and treat the solvent as point dipoles with a repulsive core which naturally excludes any differentiation between cations and anions of the same size. The equilibrium correlations are calculated within the mean spherical approximation. Details of the experimental solvent response are introduced parametrically and lead to good agreement with experimental cation mobilities in water and alcohol.

Simple continuum,⁵⁻⁹ point dipole,¹³ or even tetrahedral models for water cannot differentiate between cation and anion mobilities because of the inherent symmetry of the model for the solvent. The shift in the mobilities of the anions with respect to the cations as a function of size can be traced to the different orientation of water in the primary solvation shell of the ions (H pointed toward anions and oxygen toward cations). The symmetry breaking of water structure by small ions on charge reversal and their effect on ion mobility was not fully appreci-

ated until recent computer studies¹⁴ using a simple point charge model (SPC/E)¹⁵ for water which has the required charge asymmetry to distinguish between cation and anion solvation.

We continue to mimic the properties of the aqueous solvent by using the same (SPC/E) model, but we also exploit the flexibility available in a computer simulation to vary the charge and size of ions arbitrarily in order to probe their effect on the hydration dynamics and the self-diffusion coefficient of the solute. In a recent study,¹⁶ these parameters characterizing an ion were treated as dynamical variables in an extended system, which enabled the free energy and entropy of hydration to be calculated as continuous functions of the charge and size. One could, through this artifice, determine absolute values of the free energy and entropy of hydration and shuttle effortlessly between hydrophobic and hydrophilic solvation states. Our simulations of the mobility, solvation structure, and dynamics reported here also vary the charge or the size, although they are not treated as dynamical variables. The hydrodynamic and dielectric contributions to the friction are probed instead by turning off the charge and determining how the friction changes as one of the solute parameters (charge or the size) is altered, keeping the other constant.

We find that the diffusion coefficient of uncharged lithium Li is larger than that of the charged Li^+ , while the neutral but bigger iodine I has a smaller diffusion coefficient than the negatively charged I^- . The reasons for this are explored further in this communication. Our simulations at zero charge also allow us to test the limits of Stokes' law for the hydrodynamic friction in water. In addition, we investigate the solvation dynamics of cations and anions to determine their variation with ion size and charge since this modulates dielectric friction. Finally our calculations of hydration numbers, residence times, and exchange kinetics of water in the solvation shells of a range of cations, anions, and fictitious (e.g., zero charge) solutes provide important information on these shells or cages and show how they correlate with ion or uncharged solute diffusion in solution. Studies of ion mobility have advanced to the point where the effects described here should be considered in future elaborations of the theory in aqueous solvents.

This paper is organized as follows: the molecular dynamics simulations of the diffusion coefficients of charged and uncharged solutes are described in section II, followed by a description of the solvation dynamics of cations and anions in water in section III. The residence times of water in the shells around the ions and the corresponding uncharged species are discussed in section IV, and are related to the structure of these shells. Section V describes the kinetics of water exchange in the shells around charged and uncharged species. We conclude with a summary and discussion of the results in section VI. The mobilities and other structural and dynamical properties are very sensitive to the details of the intermolecular potentials, and our results are presented in tables and figures to provide a convenient reference for further study and elaboration of the model and theory of ion mobility.

II. Computer Simulation of Self-Diffusion of Charged and Uncharged Solutes

We calculated the mobilities of the alkali metal ions (Li^+ , Na^+ , K^+ , Rb^+ , I^+ , and Cs^+), the halides (F^- , Cl^- , Br^- , and I^-), and calcium (Ca^{2+}) at 25 °C through molecular dynamics (MD) simulations¹⁴ using the SPC/E model¹⁵ for water and ion-water parameters (Table 1) fitted to the binding energies of small clusters of ions by Dang et al.¹⁷⁻²⁴ The pair potential between

TABLE 1: Halide–Water, Alkali Metal Cation–Water, and Water–Water Potential Parameters (SPC/E Model)^a

ion/water	σ_{io} (Å)	ϵ_{io} (kJ/mol)	charge (q)	ref
F ⁻	3.143	0.6998	-1	17
Cl ⁻	3.785	0.5216	-1	19
Br ⁻	3.854	0.5216	-1	23
I ⁻	4.168	0.5216	-1	18
Li ⁺	2.337	0.6700	+1	24 ^b
Na ⁺	2.876	0.5216	+1	22
K ⁺	3.250	0.5216	+1	22
Rb ⁺	3.348	0.5216	+1	22
Cs ⁺	3.526	0.5216	+1	20, 21
Ca ²⁺	3.019	0.5216	+2	25

SPC/E	σ_{oo} (Å)	ϵ_{oo} (kJ/mol)	charge (q)	ref
O(H ₂ O)	3.169	0.6502	-0.8476	15
H(H ₂ O)			+0.4238	

^a In the SPC/E model for water, the charges on H are at 1.000 Å from the Lennard-Jones center at O. The negative charge is at the O site, and the HOH angle is 109.47°. ^b The Li⁺ parameters are for the revised polarizability (RPOL) model.

water and the ion has the form

$$\phi_{iw} = 4\epsilon_{io} \left[\left(\frac{\sigma_{io}}{r_{io}} \right)^{12} - \left(\frac{\sigma_{io}}{r_{io}} \right)^6 \right] + \sum_{j \in w} \frac{q_i q_j}{r_{ij}} \quad (2.1)$$

where ϵ_{io} and σ_{io} are Lennard-Jones parameters between oxygen on a water molecule and an ion i , q_j is the charge at site j in water, and q_i is the charge on ion i . Also, r_{io} and r_{ij} are the distances between ion i and an oxygen site of a water molecule and between ion i and a charge site j in water.

Each simulation was in the NVT ensemble with the water density fixed at 0.997 g/cm³ and the temperature at 298.15 K. The number of water molecules, except as noted below, was 215, which corresponds to a box length of 18.64 Å. Gaussian kinetics was used to control the temperature, and a quaternion formulation was employed to solve the equations of rotational motion about the center of mass of rigid SPC/E water molecules. A fifth-order predictor–corrector algorithm with a time step of 1 fs served to integrate the equations of motion.

Each system consisting of an ion and solvent molecules was equilibrated over 500 000 time steps (500 ps). Production runs consisted of a further 500 000 time steps after equilibration. Unlike our previous studies, we use a reaction field correction to account for the long-range Coulomb interactions between the charges,

$$U_{\text{coul}}(r_{ij}) = \frac{q_i q_j}{r_{ij}} \left\{ 1 + \left(\frac{\epsilon_{\text{RF}} - 1}{2\epsilon_{\text{RF}} + 1} \right) \frac{r_{ij}^3}{R_c^3} \right\} \quad (2.2)$$

where ϵ_{RF} is the dielectric constant surrounding the cutoff sphere of radius R_c , which is half the length of the simulation box. The corresponding force between the charges is obtained by differentiation with respect to r_{ij} . The ratio $(\epsilon_{\text{RF}} - 1)/(2\epsilon_{\text{RF}} + 1) = 0.5$ for $\epsilon_{\text{RF}} = \infty$; we used $\epsilon_{\text{RF}} \approx 22$, which corresponds to 0.47 for this ratio, which is not sensitive to the value of ϵ_{RF} provided it is sufficiently large. The reaction field correction is of course more easily programmed and uses less computational time than Ewald sums for the long-range charge interactions. It provides an accurate alternative to Ewald sums provided the parametrization of the potential functions is consistent with the boundary conditions used.²⁶ This is not the case in our simulations since the ion–water potentials were parametrized by fitting them to the binding energies of small

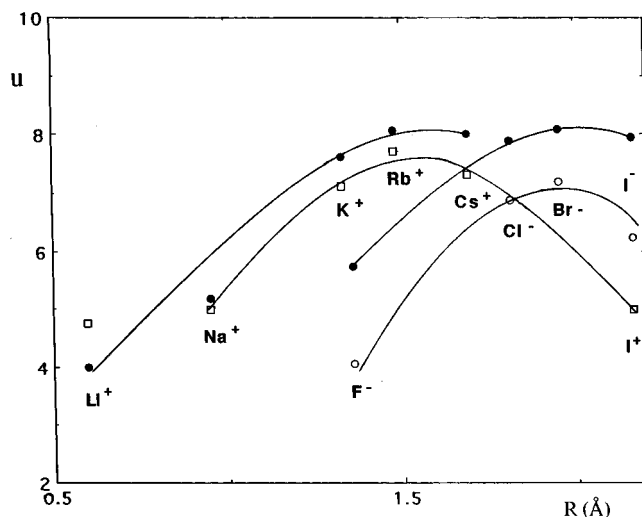


Figure 1. Ion mobilities in units of $10^{-8} \text{ m}^2 \text{ V}^{-1} \text{ s}^{-1}$ as a function of the crystallographic radius R (Å) calculated from the mean square displacement of the anions (○) and the cations (□), respectively in SPC/E water using a reaction field for the long-range Coulomb interactions. The experimental values are depicted as dark circles (●).

clusters of the solvated ion,^{17–24} but this should not seriously impair our conclusions about the relative changes in the solvation properties or mobilities for the range of cations and anions studied by us.

We have added I⁺ to the list of simulated ions to extend the size of the cations investigated; it has the same ion–water parameters as I⁻ in Table 1 except for the positive charge. Additional simulations for the sodium ion Na⁺ and the largest solutes (I⁻ and I; see below) with 511 water molecules were undertaken at the same temperature and density to assess the effect of system size on the dynamical properties of the solute and the solvent. The box length in this instance is 33% larger (≈ 24 Å) and the properties of Na⁺, I⁻, and I were unaffected, within the errors of our simulation, on increasing the system size. As shown by us¹⁶ and by Hummer, Pratt, and Garcia,²⁷ the long-range corrections influence the energy, but as seen here, they seem to have less effect on the dynamics. Equation 1.3 implies that the dielectric friction on an ion falls off rapidly with its size and the system size may have less effect on the dynamics of large ions provided it is big enough to accommodate the solvation shells. Our calculations show that the system size in our simulations is also large enough to characterize the dynamics of small ions and their hydration shells.

The ion mobilities were determined from the diffusion coefficients D_i through the Einstein relation $u_i = D_i/kT$, where k is Boltzmann's constant and T is the absolute temperature. The ion diffusion coefficients obtained independently from the mean square displacement (MSD) and the velocity autocorrelation functions (VAC) are collected in Table 2. In Figure 1 the experimental mobilities plotted as a function of the crystallographic radii in angstroms (Å) are represented as black circles and the MSD simulations are represented by open circles or squares. These calculations demonstrate that cation and anion mobilities fall on separate curves, as functions of ion size, with distinct maxima. This is qualitatively in accord with experiment, although the agreement between experimental anion mobilities is slightly worse than the corresponding results obtained earlier without the reaction field corrections.¹⁴ This may be due to the fact that the ion–water model parameters were determined from the equilibrium properties of small ion–water clusters or because the SPC/E model tends to exaggerate the cation–anion difference.

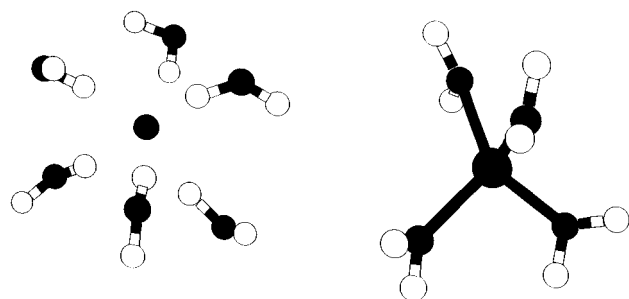


Figure 2. Primary hydration shells of Li^+ and F^- ions. The water molecules are approximately tetrahedrally oriented around Li^+ with O atoms near the ion, while F^- has approximately 6–7 water molecules around it with protons near the ion.

TABLE 2: Diffusion Coefficient D and Mobilities u of Solutes at Infinite Dilution in Water at 25 °C Calculated from the Mean Square Displacements and Velocity Autocorrelation Functions

ion	$D(10^{-9} \text{ m}^2 \text{ s}^{-1})$		$u(10^{-8} \text{ m}^2 \text{ V}^{-1} \text{ s}^{-1})$	
	MSD	VAC	MSD	VAC
F^-	1.04 ± 0.06	0.99 ± 0.08	4.04 ± 0.23	3.85 ± 0.31
F	3.31 ± 0.20	3.21 ± 0.21	12.88 ± 0.78	12.49 ± 0.82
Cl^-	1.77 ± 0.08	1.65 ± 0.02	6.88 ± 0.31	6.42 ± 0.08
Cl	1.51 ± 0.13	1.60 ± 0.11	5.88 ± 0.51	6.23 ± 0.43
Br^-	1.85 ± 0.18	1.76 ± 0.06	7.20 ± 0.70	6.85 ± 0.23
Br	1.30 ± 0.08	1.29 ± 0.05	5.06 ± 0.31	5.02 ± 0.19
I^-	1.60 ± 0.01	1.61 ± 0.05	6.23 ± 0.04	6.27 ± 0.19
I	0.98 ± 0.05	1.00 ± 0.02	3.81 ± 0.19	3.89 ± 0.08
I^+	1.28 ± 0.12	1.23 ± 0.12	4.98 ± 0.47	4.79 ± 0.47
Li^+	1.22 ± 0.02	1.18 ± 0.01	4.75 ± 0.08	4.59 ± 0.04
Li	14.35 ± 0.40	15.85 ± 0.57	55.85 ± 1.56	61.69 ± 2.22
Na^+	1.28 ± 0.05	1.29 ± 0.06	4.98 ± 0.19	5.02 ± 0.23
Na	5.42 ± 0.10	5.73 ± 0.19	21.10 ± 0.39	22.30 ± 0.73
K^+	1.83 ± 0.13	1.85 ± 0.10	7.12 ± 0.51	7.20 ± 0.39
K	2.60 ± 0.05	2.71 ± 0.20	10.12 ± 0.19	10.55 ± 0.78
Rb^+	1.98 ± 0.08	1.91 ± 0.02	7.71 ± 0.31	7.43 ± 0.08
Rb	2.08 ± 0.02	2.11 ± 0.27	8.10 ± 0.08	8.21 ± 1.05
Cs^+	1.88 ± 0.17	1.89 ± 0.15	7.32 ± 0.66	7.36 ± 0.58
Cs	2.03 ± 0.01	1.94 ± 0.04	7.90 ± 0.04	7.55 ± 0.16
Ca^{2+}	0.53 ± 0.03	0.55 ± 0.01	2.06 ± 0.12	2.14 ± 0.04

As stated in the Introduction, the shift in the mobilities of the anions with respect to the cations (Figure 1) can be traced to the different orientation of water (Figure 2) in the primary solvation shell of the ions (H pointed toward anions and oxygen toward cations) in the SPC/E model and its effect on the friction. A molecular theoretical treatment that takes this into account in calculations of ion mobility has yet to be worked out. The velocity autocorrelation function of the ions shown in Figure 3 depicts a gradual change from oscillatory to monotonic decay as the ions grow larger. The mean square displacements of the ions are shown in Figure 4.

We also calculated the diffusion coefficients of nonpolar solutes using the same model for water and the ions of Table 1 except that the charges are turned off. They are summarized in Table 2, and Figure 5 shows the dramatic effects of charge neutralization on the diffusion coefficients. The mobilities, defined as $u_i = D_i/kT$, of the discharged Li, Na, K, Rb, and F are larger than the corresponding results for the charged ions, whereas the calculated values for Cl, Br, and I lie below the mobilities of the corresponding anions. The diffusion coefficient of Cs^+ shows the smallest change on discharging the ion. These results immediately suggest that the variation in the mobility with charge and size is somehow related to the structure of the solvent around the ions characterized by the entropy and free energy of solvation and by the solvation dynamics which we describe in the next section. A plot of the friction coefficient of the uncharged species vs the radius taken as σ_{iO} of Table 1

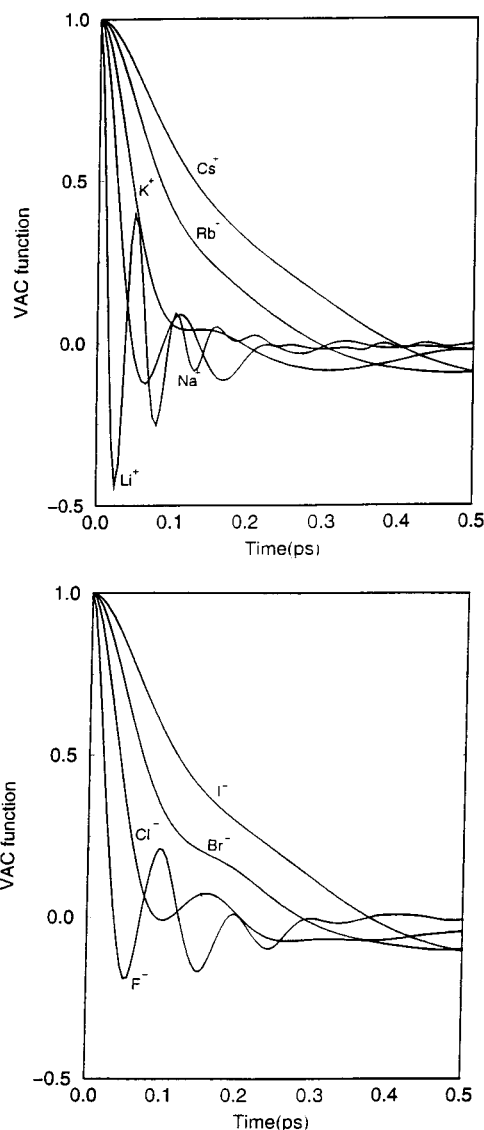


Figure 3. Velocity autocorrelation functions of positive and negative ions as functions of time (in ps). Note the oscillations of the small ions in their solvation shells.

(Figure 6) is approximately linear. Assuming slip boundary conditions and Stokes' law the viscosity of SPC/E water at 25 °C is calculated to be $1.73 \times 10^{-3} \text{ kg m}^{-1} \text{ s}^{-1}$. The experimental value for water at this temperature is $0.89 \times 10^{-3} \text{ kg m}^{-1} \text{ s}^{-1}$.

The ion oxygen $g_{iO}(r)$ and ion hydrogen $g_{iH}(r)$ radial distribution functions have been discussed earlier¹⁴ for the same set of ions except I^+ and Ca^{2+} . The distribution functions for the uncharged species are shown in Figure 7, and the positions of the maxima and minima of the solute–oxygen $g_{iO}(r)$ functions are collected together with the corresponding results for the ions in Table 3.

Figure 8 compares solute oxygen distribution functions $g_{iO}(r)$ for I^- , I, and I^+ and shows that the water molecules are drawn closer toward I^- than toward I^+ . The ion–oxygen distribution function for the Ca^{2+} ion (Figure 9) is sharply peaked and has a low minimum between the first and second hydration shells like the distribution functions for Li^+ (Table 3), indicating a tightly bound first shell of water molecules.

III. Solvation Dynamics of the Ions

The dynamical response of a solvent to charge perturbation has been studied extensively over the past decade in time-

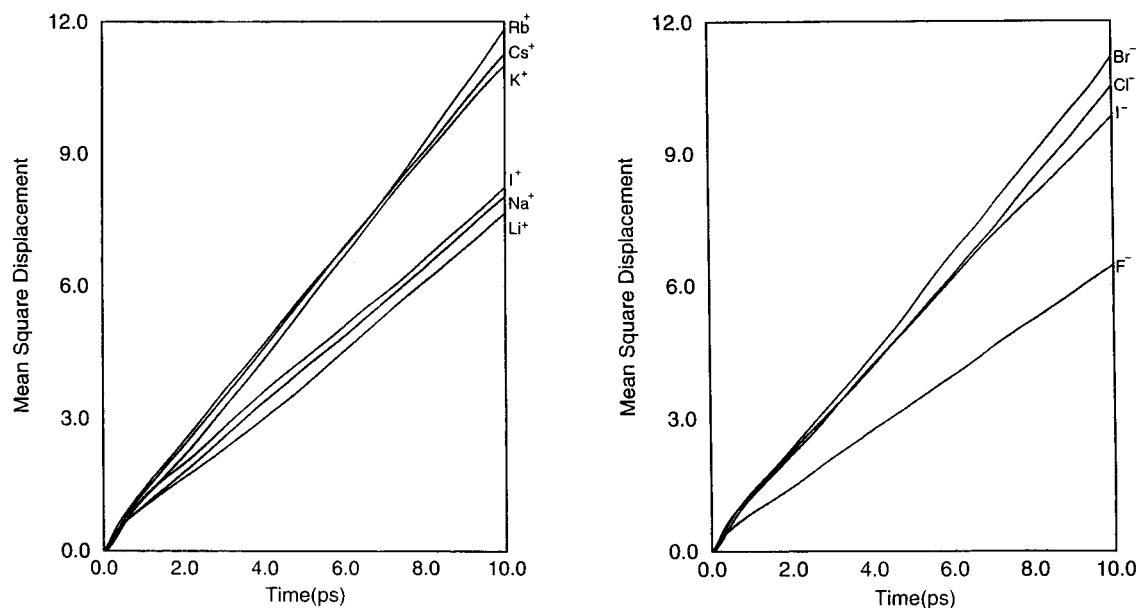


Figure 4. Mean square displacement of the cations and anions in units of \AA^2 .

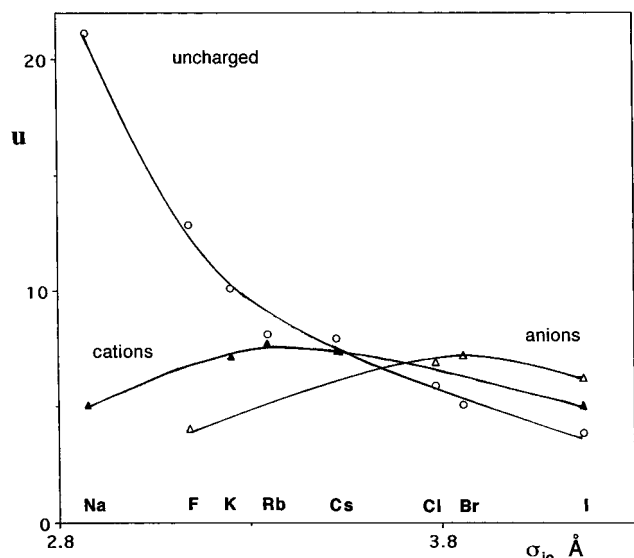


Figure 5. Mobilities of charged and uncharged species as a function of the radii.

delayed fluorescence experiments^{28,29} and by computer simulation.^{30–38} Its effect on fast chemical reactions such as electron transfer, cis–trans isomerization and photochemical reactions in solution has been widely appreciated.^{39–47} The mobility of an ion may be considered as a response to an external electric field, and it is influenced by the energy and dynamics of solvation, which could retard or even enhance its mobility. Although solvation dynamics is often characterized as a solvent property (e.g., through one or more relaxation times or a characteristic fast response at short times),²⁹ its dependence on the solute probe has been appreciated only recently.³⁵ We investigate this aspect of solvation dynamics for our model cations and anions in SPC/E water.

The solvent response is defined by

$$S(t) = [E(t) - E(\infty)]/[E(\infty) - E(0)] \quad (3.1)$$

where $E(t)$ is the ion–solvent energy of interaction at time t after the charges are turned on in an equilibrated system containing the uncharged solute. We consider a single ion in

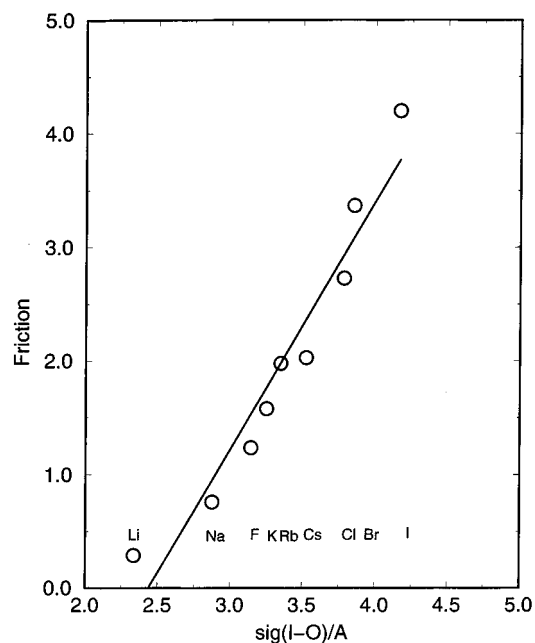


Figure 6. Friction coefficient (kg s^{-1}) vs size σ_{oi} (\AA) for the uncharged species. This shows that Stokes law is obeyed reasonably well.

SPC/E water, and our simulations of $S(t)$ for different ions are shown in Figures 10 and 11. Each of the curves indicates a rapid decline in $S(t)$ on a femtosecond time scale, followed by an oscillatory decay and slower long time relaxation. The initial drop in $S(t)$ during the first few femtoseconds is larger for cations than for anions, but the oscillatory response following this is similar for both types of ions and has a frequency of about 26 ps^{-1} . The amplitude of the oscillations depends on the solute size for a given charge and is greater for the larger ions. The period of oscillation is weakly dependent on the charge and size, but the long time decay is essentially the same for solutes of either charge, making it a characteristic of the solvent. By fitting this decay to an exponential, we find a solvent relaxation time of about 0.34 ps. The initial fast response of the solvent, modulated by the solute charge and size, could be attributed to the rotational and translational rearrangement of the solvent on charging up the solute. The

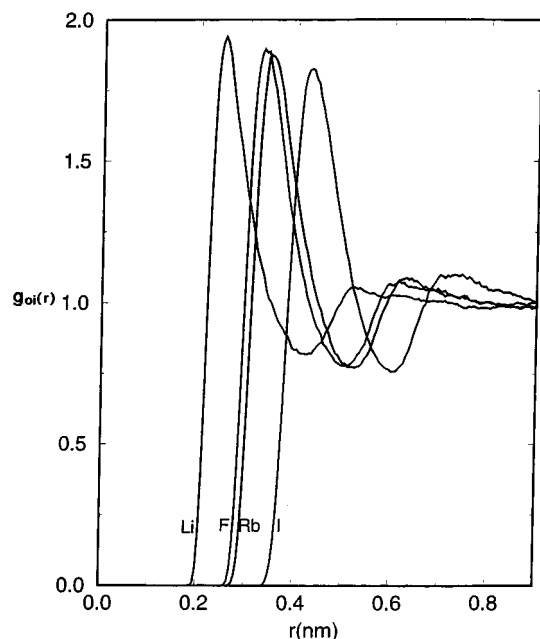


Figure 7. Solute-oxygen radial distribution functions of uncharged Li, Rb, F, and I.

TABLE 3: Positions and Magnitudes at Maxima and Minima of Solute-Oxygen g_{io} and Oxygen-Oxygen Radial Distribution Functions g_{oo} at 25 °C

ion	first max		first min		second max		second min	
	$r_{io}/\text{Å}$	g_{io}	$r_{io}/\text{Å}$	g_{io}	$r_{io}/\text{Å}$	g_{io}	$r_{io}/\text{Å}$	g_{io}
F ⁻	2.60	7.92	3.20	0.17	4.45	1.45	5.50	0.79
F	3.34	1.88	5.05	0.78				
Cl ⁻	3.20	4.06	3.80	0.49	5.00	1.28	6.05	0.89
Cl	3.89	1.88	5.65	0.74				
Br ⁻	3.30	3.46	3.85	0.52	5.05	1.23	6.15	0.88
Br	4.01	1.87	5.73	0.73				
I ⁻	3.60	2.68	4.30	0.72	5.05	1.25	6.65	0.85
I	4.25	1.81	6.03	0.73				
I ⁺	3.83	2.10	5.85	0.87				
Li ⁺	1.95	14.00	2.65	0.02	4.10	1.69	5.25	0.89
Li	2.50	1.94	4.15	0.81				
Na ⁺	2.45	7.21	3.25	0.16	4.50	1.42	5.40	0.84
Na	2.97	1.90	4.76	0.80				
K ⁺	2.80	4.57	3.65	0.47	4.75	1.15	5.80	0.90
K	3.39	1.88	5.09	0.77				
Rb ⁺	2.90	3.94	3.75	0.59	5.10	1.14	5.90	0.89
Rb	3.49	1.87	5.23	0.76				
Cs ⁺	3.05	3.20	3.85	0.74	5.40	1.09	6.25	0.90
Cs	3.53	1.85	5.25	0.76				
Ca ²⁺	2.45	14.14	3.39	0.01	4.46	1.96	5.43	0.79
Ca	3.15	1.93	4.85	0.76				

water	$r_{oo}/\text{Å}$	g_{oo}	$r_{oo}/\text{Å}$	g_{oo}	$r_{wo}/\text{Å}$	g_{oo}	$r_{oo}/\text{Å}$	g_{oo}
H ₂ O	2.75	2.98	3.30	0.83	4.50	1.10	5.65	0.90

oscillatory response is more likely a reflection of the rotational reorientation of the solvent molecules accompanied by librational motion with an amplitude that is greater for larger ions because of the weaker electric field in the solvent shells.

IV. Hydration Numbers and Residence Times

The residence times of water in the solvation shells and the corresponding hydration numbers provide information about the lifetime and population of the solvent molecules near an ion or an uncharged solute. How this depends on the charge and the size of the solutes is of interest in relation to the diffusion coefficients described in section II.

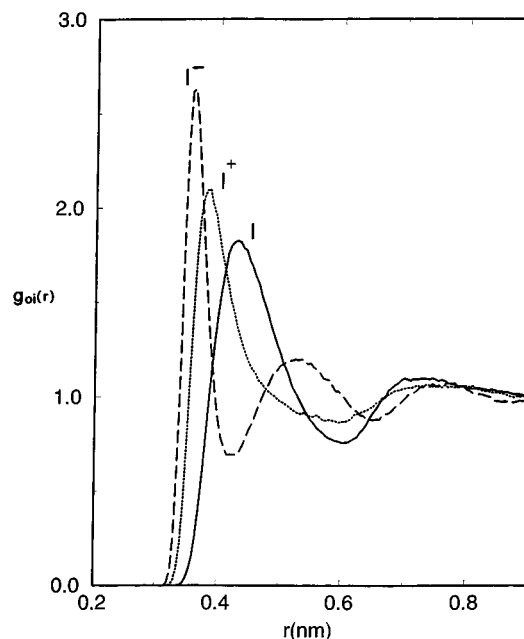


Figure 8. Ion-oxygen radial distribution functions of I⁻, I⁺, and I.

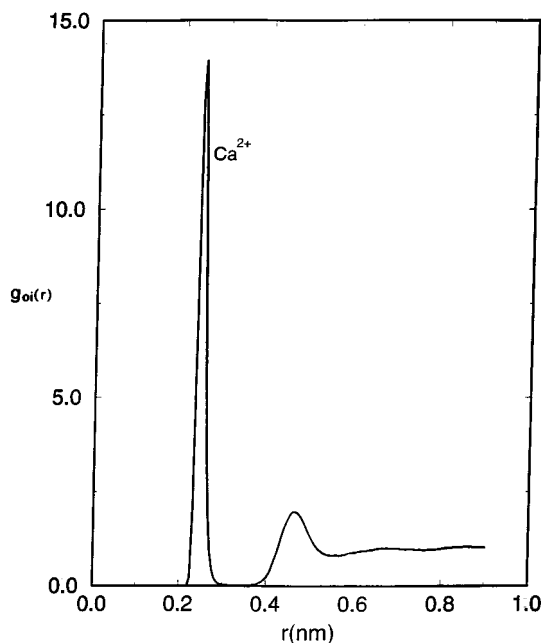


Figure 9. Ion-oxygen radial distribution function of Ca²⁺. Note the deep minimum, indicating a tightly bound first hydration shell.

The hydration number N_h in the primary shell was calculated from the solute-oxygen distribution functions $g_{io}(r)$ using

$$N_h = \int_0^{R_1} g_{io}(r) 4\pi r^2 dr \quad (4.1)$$

where the upper limit of integration R_1 is the radius of the first hydration sphere which corresponds to the first minimum in $g_{io}(r)$. Integration between R_1 and the second minimum R_2 in the distribution function $g_{io}(r)$, when it exists, provides the hydration numbers in the second shell. A second shell is identified only for the charged species (except Cs⁺) and a third shell is also clearly visible in the ion-water distribution functions of most anions but not cations. The water molecules in the primary shell of a negative ion have H pointed toward the ion and are drawn closer toward the ion than water molecules in the primary shell of a positive ion of the same size which

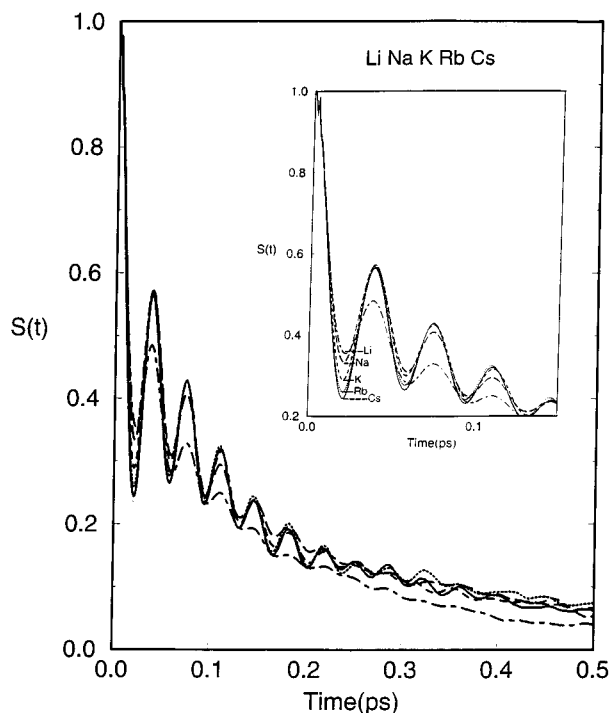


Figure 10. Response function (eq 3.1) of the cations as a result of switching on the charge. Inset shows the response function at short times. Note the variations in the oscillations at short times and the similar response at long times except for Li^+ .

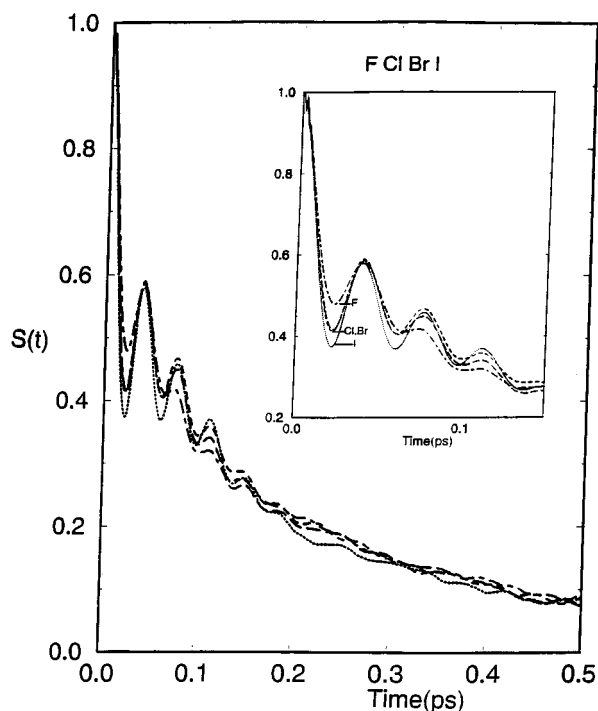


Figure 11. Response function (eq 3.1) of the anions as a result of switching on the charge. Inset shows the response function at short times. Note the variations in the oscillations at short times and the similar response at long times.

has oxygen pointed toward the ion. Figure 8, which compares $g_{io}(r)$ for I^- , I , and I^+ , shows this clearly. The hydration numbers in the primary shells of the three solutes vary widely from 7.9 for I^- to 27 for I and 25 for I^+ .

Hydration numbers listed in the second column of Table 4 are plotted as a function of the shell size in Figure 12. The number of water molecules in the primary hydration shell varies

TABLE 4: Average Coordination Numbers and Residence Times (ps) of Water in Hydration Shells of an Ion and the Corresponding Discharged Species in SPC/E^a Water at 25 °C

ion	hydration number	res time ps* num (expon fit)	res time ps num (expon fit)
F^- (1st shell)	6.3	24.5(24.5)	23.4(23.7)
F^- (2nd shell)	19.4	14.5(15.1)	10.4(11.8)
F	17.1	19.3(20.1)	15.5(17.6)
Cl^-	7.2	16.6(17.5)	12.8(14.0)
Cl	22.6	23.0(24.1)	13.4(15.6)
Br^-	7.5	22.2(22.8)	18.2(19.9)
Br	26.5	13.2(13.6)	11.3(12.4)
I^-	23.1	20.4(21.3)	14.8(16.9)
I	23.1	25.6(26.2)	19.0(20.6)
I^+	7.9	13.8(14.9)	8.9(10.3)
Li^+	29.5	24.7(26)	13.7(16.2)
Li	27.2	27.9(28.2)	23.7(25.2)
Na^+	25.1	21.4(21.8)	19.0(20.5)
Na	4.1	50.6(50.6)	54.4(54.5)
K^+	17.4	16.19(16.5)	11.2(12.7)
K	11.0	7.7(9.3)	4.1(6.9)
Rb^+	5.8	22.4(22.8))	19.6(19.8)
Rb	18.3	18.2(19.2)	11.9(13.8)
Cs^+	12.6	12.9(13.5)	8.7(10.3)
Cs	7.1	14.3(15.1)	8.7(9.4)
Ca^{2+}	19.4	18.6(19.8)	9.7(12.1)
Ca	17.6	17.9(18.7)	14.1(16.4)
$\text{H}_2\text{O}(\text{SPC}/\text{E})$	7.9	12.1(12.6)	10.0(11.5)
	21.0	16.3(17.4)	10.2(12.7)
	19.3	20.0(20.5)	16.4(18.2)
	8.3	13.9(14.8)	10.1(11.6)
	19.5	19.9(20.2)	15.7(17.2)
	7.9	699(699)	700(700)
	17.6	18.7(18.9)	16.7(16.7)
	15.7	13.6(14.2)	9.9(11.5)
	4.4	5.7(6.9)	5.20(6.6)

^a The second solvation shell for Cs^+ and all the uncharged species is not clearly defined. Data for this are not presented in the table.

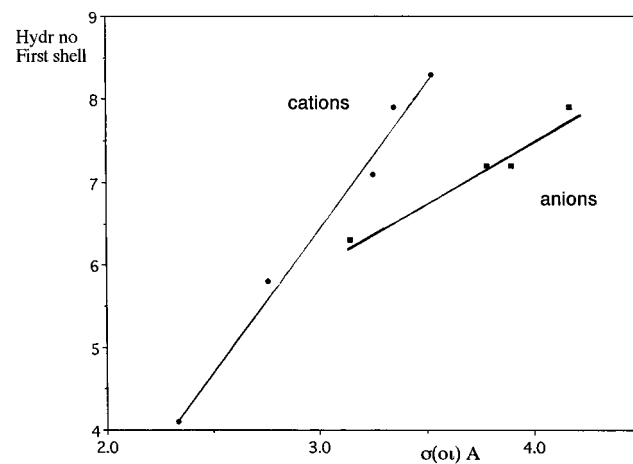


Figure 12. Hydration numbers of the first solvation shell of ions as a function of the shell radius.

linearly with the size but with different slopes for cations and anions. The hydration numbers of the discharged ions approach the number of water molecules in the second shell of the corresponding charged ions from below as the ions become larger. These results are easily understood in terms of the charge asymmetry of water molecule and the decrease in the field with ion size. However, the residence times of the water molecules in these shells are more interesting since they are correlated with the increase or decrease in the diffusion coefficients on charge neutralization.

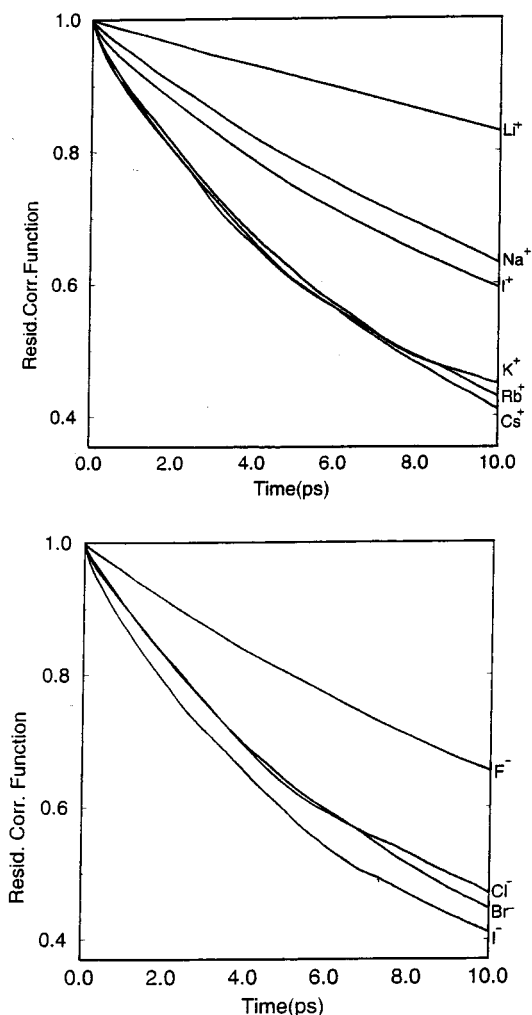


Figure 13. Residence correlation functions for the hydrated water molecules in the first solvation shell of cations and anions.

The residence times are calculated from time correlation functions^{15,22} defined by

$$R(t) = \frac{1}{N_h} \sum_{i=1}^{N_h} [\theta_i(0) \theta_i(t)] \quad (4.2)$$

where $\theta_i(t)$ is the Heaviside unit step function, which is 1 if a water molecule i is in the coordination shell of the ion at time t and zero otherwise, and N_h is the hydration number of this shell. Following Impey et al.,⁴⁸ we allow for the temporary excursion of water from a hydration shell by counting it as present if it is only absent for period $t^* \leq 2$ ps. This may change $R(t)$ at short times (< 2 ps), but it does not noticeably affect the residence times of water in the primary hydration shells of the smaller ions, which are much larger than 2 ps. It does however change the residence times of the secondary hydration shells of the ions and more noticeably the residence times of water in the (primary) shells of the uncharged species! Excursions of water molecules from these shells are thus more frequent, implying rapid crossing and recrossing in and out of the shell. The time correlation functions and residence times of the hydration shells assuming the 2 ps delay are labeled with an asterisk in Table 4.

Figure 13 displays the time dependence of the ensemble-averaged $\langle R(r,t) \rangle$ for water around the anions and cations

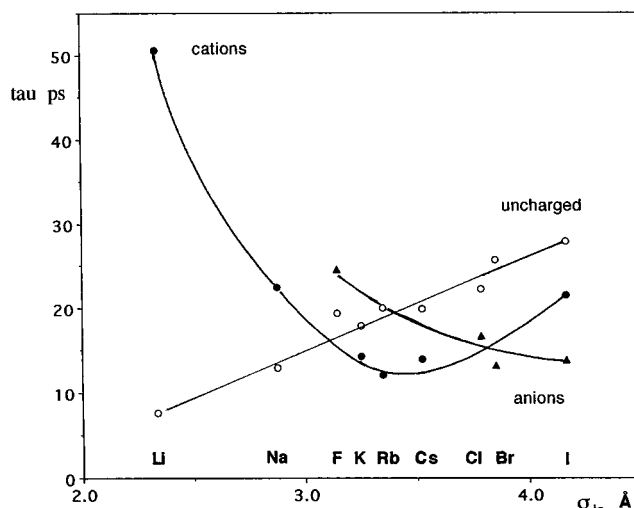


Figure 14. Residence times of cations, anions, and uncharged species as a function of the solute size.

calculated in our simulations. The residence time, τ , is defined by

$$\tau = \int_0^{\infty} \langle R(t) \rangle dt \quad (4.3)$$

but was obtained by numerical integration of $\langle R(t) \rangle$ up to $t = 10$ ps, with the remainder calculated by fitting $\langle R(t) \rangle$ at large times to an exponential decay $e^{-t/\tau}$. The residence times τ are summarized in Table 4; the numbers in parentheses are τ' that would be equal to the actual residence time if $\langle R(t) \rangle$ decayed exponentially with a single characteristic time τ' for long and short times. The two residence times are labeled “num” (for numerical) and “expon fit” (for exponential fit) at the heads of the columns. Simulations of Na^+ with 512 water molecules lead to residence times within 2 ps of those for this ion reported in Table 4. We consider this as an approximate measure of the accuracy of the times given in Table 4.

Figure 14 shows that the residence time of water in the first shell generally decreases or increases with the size σ_{i0} of the shell depending on whether the solute is charged or uncharged. The exception to this is the increase in the residence time from Rb^+ through Cs^+ to the fictitious I^+ . The residence time minimum correlates nicely with the maximum in the solvation entropy of cations as a function of the size determined by Lynden-Bell and Rasaiah^{16a} (Figure 4 of ref 16a). Allowing for a 2 ps excursion time and differences in the shell radii, the residence times of water molecules in the second shell of the large ions and the primary shell of the corresponding uncharged solutes are similar. With some exceptions (notably lithium, sodium, and fluorine) the residence time of water in the first hydration shell of a discharged solute is larger than the residence time of water in the primary shell of the corresponding charged ion. Remarkably, the large residence time of 28 ps for water in the first shell of uncharged iodine I is halved when it acquires a negative charge but decreases only slightly to 21 ps when it acquires a positive charge (I^+). This is in sharp contrast to the residence time of 8 ps for water in the primary shell of uncharged lithium Li, which increases by a factor of 6 when Li is charged to Li^+ .

The conclusion is inescapable that the water molecules in the primary solvation sheaths around smaller positive and negative ions are not only oriented differently, with respect to the ion, due to the charge asymmetry of water, but they are also structurally different from the solvation of large uncharged solutes and cations (e.g., I^+). Stereoscopic pictures (Figure 15)

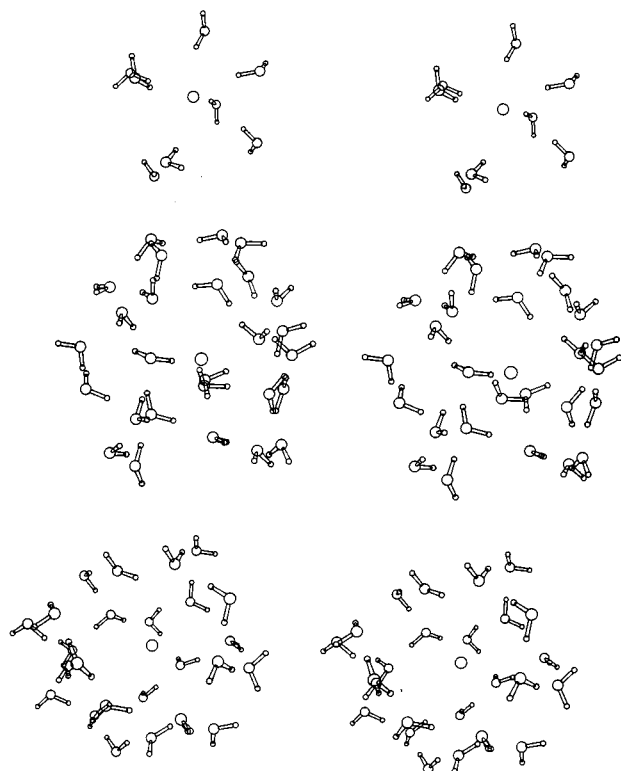


Figure 15. Stereoscopic picture of the equilibrium configuration of the first solvation cage of water molecules around uncharged I^- , I , and I^+ from top to bottom.

confirm that the solvent molecules near an uncharged I or I^+ in SPC/E water form a cage around the solute in contrast to the water molecules oriented toward the ion in the primary shell around I^- . This is consistent with the entropies of solvation calculated as a function of the charge by Lynden-Bell and Rasaiah, who introduced the terms hydrophobic and hydrophilic solvation.^{16a} The uncharged solute has the lower entropy of solvation (hydrophobic solvation), and the increase in the solvation entropy on charging I to I^+ is less than the increase when I is charged to I^- . The asymmetry in the solvation entropy on charge reversal diminishes as the size of the solute decreases (Figure 4 of ref 16a) and is correlated with the asymmetry in the residence times of water in the primary shells of I^+ and I . It also appears to be correlated with the asymmetry in the dynamical properties such as the mobility of positive and negative ions in aqueous solutions at 25 °C. The increased mobility of I^- as compared to I is related to the collapse of the solvent cage enclosing I when it is charged to I^- .

V. Solvent Exchange and Hydrogen Bond Dynamics

We expect the different types of hydrophobic and hydrophilic solvation to be reflected in the exchange dynamics of the water in the primary shell around the positive and negative ions as well as uncharged solutes. Rey and Hynes^{49,50} describe the detailed dynamics in simulations of water exchange around a Na^+ at room temperature in terms of unimolecular S_N1 and bimolecular exchange S_N2 reactions and also concerted exchanges in which several molecules enter and leave the shell more or less simultaneously. We find that apart from the behavior observed by Rey and Hynes in the primary shells of Na^+ , the dynamics of the secondary shell around singly charged ions and the primary shell water encircling an uncharged solute or large charged ion (I^+) is more strongly influenced by the interactions between water molecules forming these cages rather than by their interaction with the caged solute.

TABLE 5: Hydration Shell Dynamics. Rate Coefficients Calculated from Residence Time τ^* Determined in MD Simulations ($k^{MD} = 1/\tau^*$) and Transition State Theory (k^{TST}) and the Corresponding Transmission Coefficients $\kappa = k^{MD}/k^{TST}$

ion	k^{MD} (ps ⁻¹)	k^{TST} (ps ⁻¹)	κ
Li^+	0.020	0.069	0.29
Na^+	0.045	0.22	0.21
K^+	0.070	0.71	0.10
Cs^+	0.072	0.95	0.08
F^-	0.041	0.24	0.17
Cl^-	0.060	0.69	0.09
Br^-	0.075	0.74	0.10
I^-	0.072	1.12	0.06

The rate coefficient for exchange is $k^{MD} = 1/\tau^*$, where τ^* is the residence time of water in the primary shell which includes the 2 ps excursion time described earlier. The free energy barrier for solvent exchange in the primary shell of an ion may be determined from the potential of average force $w_{io}(r)$ between the ion and a surrounding water molecule. It is related to the orientationally averaged ion–water distribution functions $g_{io}(r)$ by $-\beta w_{io}(r) = \ln g_{io}(r)$, where $\beta = 1/kT$ in which k is Boltzmann's constant and T is the absolute temperature. Figure 16 displays this for cations and anions. From a simple unimolecular perspective the reaction coordinate for exchange is the ion–water distance. The free energy change as a function of the ion–water distance r is obtained by adding a term describing the increase in volume with r and is given by

$$\beta w_{io}^{eff}(r) = \beta w_{io}(r) - 2 \ln(r/r^\#) \quad (5.1)$$

where $r^\#$ corresponds to the top of the barrier. Figure 17 shows this for Li^+ and K^+ ions. The barrier for dissociation of the ion–water pair varies from 6 to 3 in units of kT from Li^+ to K^+ and $4kT$ to $2kT$ from F^- to Br^- . The rate coefficient is $k^{MD} = \kappa k^{TST}$, where κ is the transmission coefficient, and the transition state theory rate coefficient,

$$k^{TST} = \left(\frac{kT}{2\pi\mu}\right)^{1/2} \frac{e^{-\beta w_{io}^{eff}(r^\#)}}{\int_0^{r^\#} dr e^{-\beta w_{io}^{eff}(r)}} \quad (5.2)$$

is an upper bound for the rate coefficient so that $\kappa \leq 1$. In eq 5.2 μ is the reduced mass of the dissociating ion–water pair in the exchange process. Our results for k^{MD} , k^{TST} , and κ are summarized in Table 5. The calculations for Na^+ agree closely with Rey and Hynes' determination, and the general conclusion is that the deviations from transition state theory are large. This could be interpreted in terms of Grote–Hynes theory⁵¹ or its extensions, which we will not pursue.⁵²

The free energy barriers calculated on the same basis for water exchange around Cs^+ , I^- , and the uncharged solutes are much smaller ($1kT$, and $1.5kT$, respectively) (see Figure 18). Yet the residence time of water in these shells is large! This suggests that the structure and dynamics of water molecules in these shells are very different from what they are in the primary shells around small cations and anions. The solvation dynamics of water in the cages around uncharged solutes are strongly influenced by the h-bonded water–water interactions within the cage, and the solute–water distance is no longer an appropriate reaction coordinate to describe the kinetics of water exchange.

To study this further in simulations of uncharged solutes in SPC/E water, we must define a h-bond between two water molecules and examine a property characteristic of this bonding such as the fluctuations in the populations of the hydrogen (h)

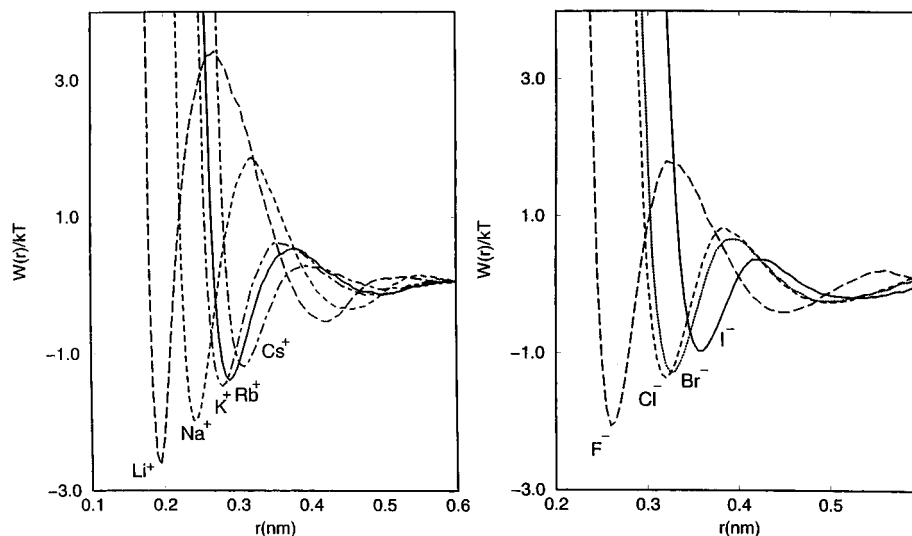


Figure 16. Ion–water potentials of average force for cations and anions as a function of the ion–water distance r .

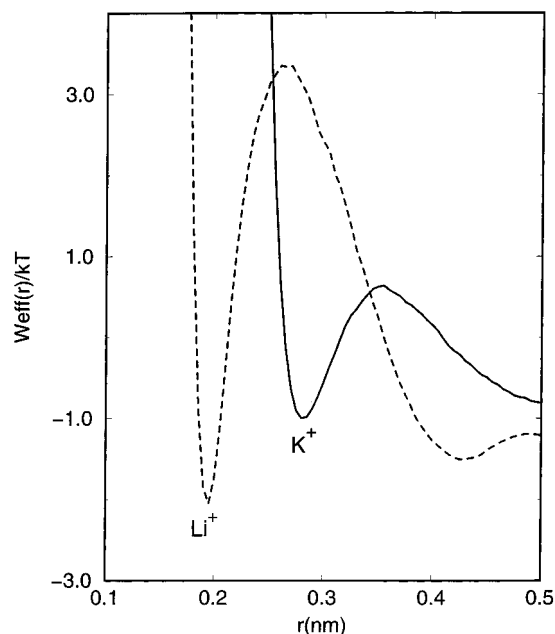


Figure 17. Effective potentials of average force for Li^+ and K^+ as a function of the ion water distance r . Note the difference between the very high barrier preventing escape of water from the shell around Li^+ and to the comparatively lower barrier for escape from the shell around the larger potassium ion. Nevertheless the residence times (51 ps for Li^+ and 14 ps for K^+) differ by a factor of only 3.5.

bonds.^{53,54} We compare this with the corresponding population fluctuations in the first hydration shell around the discharged solute, e.g., iodide (I). Two water molecules are considered to be h-bonded if their interoxygen distance is less than 3.29 Å and simultaneously the O–H...O angle is less than 30°. Following Luzar and Chandler,^{53,54} we define a hydrogen bond population operator $h(t)$, which is 1 if the pair of waters is h-bonded and zero otherwise. Fluctuations in the hydrogen bond populations are characterized by the correlation function

$$C(t) = \langle h(t)h(0) \rangle / \langle h \rangle \quad (5.3)$$

which is the conditional probability that a hydrogen bond is intact at time t if it existed at zero time. Here $\langle \rangle$ signifies an ensemble average, and the average number of h-bonds is $N(N-1)\langle h \rangle/2$, where N is the hydration number or the number of bulk waters depending on the region of interest. Luzar and

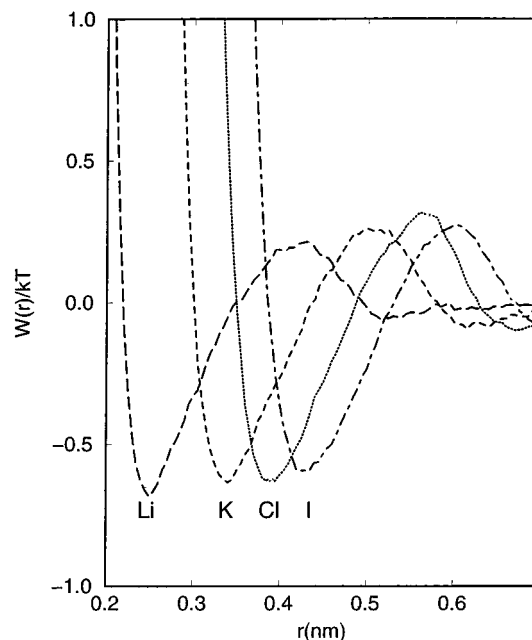


Figure 18. Potentials of average force for uncharged Li, K, Cl, and I as a function of the solute–water distance. The barrier heights are essentially the same but the residence times for water in the first shell or cage vary from 7.7 ps for Li to 28 ps for I.

Chandler relate the detailed h-bond dynamics of SPC water with the time derivative $dC(t)/dt$.

We have calculated $C(t)$ for bulk SPC/E water, for the water in the primary hydration shells of uncharged I, and for a water molecule treated as a solute in bulk SPC/E water. For the last two “solutes” only h-bonding within the primary shell is considered and h-bonding with water outside the shell is excluded. The correlation functions computed in our simulations at room temperature are shown in Figure 19.

The population fluctuations of h-bonded molecules in the shell around the uncharged I are similar to those observed in bulk water but quite different from the h-bond fluctuations within the first “hydration shell” around a single water molecule in the bulk fluid. The implied presence of a fluctuating hydrogen-bonded cage around uncharged I is clear from Figure 19. It is consistent with the lowering of the solvation entropy accompanying charge neutralization of I^- or I^+ in SPC/E water observed in simulations by Lynden-Bell and Rasaiah.^{16a}

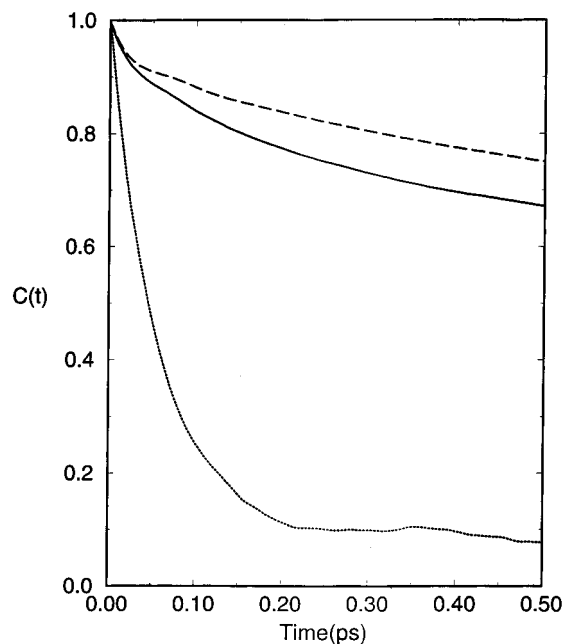


Figure 19. The hydrogen bond correlation function $C(t)$ given by eq 5.3 for bulk water (dashed line), water in the first solvation shell or cage around uncharged I (solid line), and water in the solvation shell around a water molecule in bulk water (dotted line).

VI. Conclusions

Our simulations of ion mobility in SPC/E water show the same trends with respect to size and charge type observed in experiments and also provide information on the solvation structure and dynamics that bear indirectly on ion mobilities in aqueous solutions. We have analyzed this further through studies of fictitious systems, with zero charge for example, that reveal some of the limitations of current theories and provide directions for future theoretical developments.

The mobility of an ion is a complicated function of its charge and size that is modulated by the structure and dynamics of the hydration shells and the solvent. This was discussed by Chen and Adelman,¹⁰ using a simple modification of the continuum model. The solvation shell around small ions is dramatically altered by charge neutralization; the changes though less drastic for a large ion with a weaker field are also qualitatively different since larger solutes appear to be encased within solvent cages with a finite lifetime determined by water–water h-bond interactions. The structure of the solvation sheaths and, to a lesser extent, their short time dynamics depend on the sign of the ionic charge since the water molecules, around cations and anions, are oriented differently in the primary hydration shells.

Our studies of the structure and dynamics of the solvation shells complement and support conclusions drawn from recent investigations of the free energy and entropy of solutes as continuous functions of their charge and size.^{16a} These studies showed that the entropy of solvation of a solute passes through a minimum near zero charge, signaling cage formation (hydrophobic hydration) with the water molecules held together by h-bonds. The solvation entropy gradually increases as the solute is charged positively or negatively, reflecting breakup of the cage. Further increase in the charge promotes ion solvation or hydrophilic hydration through electrostatic ion–water interactions and leads eventually to a decrease in the solvation entropy after passing through maxima on either side of the entropy minimum. The asymmetry in the entropy–charge curves implies that the hydrophilic entropy of solvation is determined

by the sign and magnitude of the ion charge and is governed by the interaction between this charge and the higher multipoles of the asymmetric charge distribution of the water molecule as well as the water dipole.

The shift in the mobilities of the anions with respect to the cations as a function of size is related to the different orientation of water molecules in the primary solvation shell of the ions (H pointed toward anions and oxygen toward cations) which arises from the charge asymmetry of the water molecule. The increased mobility of the lithium ion on discharge is understood in terms of an effective decrease in size of the moving entity due to desolvation. In contrast to this, the decreased mobility of the iodide ion (I^-) on charge neutralization arises from solvent cage formation. The cage breaks up, leading to greater mobility when I is charged to I^- . This is accompanied by a decrease in coordination number from 27 to 8, a decrease in the residence time from 28 to 14 ps, and an increase in the solvation entropy as observed in simulations by Lynden-Bell and Rasaiah.^{16a} In contrast to this, the coordination number and residence time decrease only slightly when I is charged to I^+ and the mobility shows a correspondingly small increase. The increase in entropy of solvation is also smaller than the increase in going from I to I^- .

The minimum in the residence times of water in the primary hydration shell around cations as a function of size correlates with the maximum in the solvation entropy, again suggesting different types of hydration for small and large cations. The lower entropy and larger water of hydration residence times associated with small cations reflect orientational ordering of the waters in the primary shell by strong ion–water interactions. Similar features of a large residence times and lower entropy of solvation observed for large cations (I^+) are however related to cage formation through h-bond interactions between water molecules forming the cage. The borderline between these extremes lies at or near the solute size corresponding to the Rb^+ ion.

The incorporation of the subtle effects of solvation dynamics, solvent caging, and charge asymmetry described here and the polarizability of ions and solvent molecules⁵⁵ not explicitly considered in this study in molecular theories of ion mobility present interesting challenges for the future.

Acknowledgment. We thank Dr. Alenka Luzar for discussions on h-bond dynamics. This research was supported by the National Science Foundation, under Grant No. CHE 9610288 to J.C.R. R.M.L.B. is supported by an EPSRC (Grant GR/LO8427) and thanks the International Fund for Ireland for support for the Irish Center for Colloid Science and Biomaterials. S.H.L. is supported by the Korea Science and Engineering Foundation and by the Nondirected Research Fund of the Korea Research Foundation.

References and Notes

- (1) Falkenhagen, H. L. *Electrolytes*; Clarendon Press: Oxford, 1934.
- (2) Onsager, L.; Fuoss, R. M. *J. Phys. Chem.* **1932**, *36*, 2689.
- (3) Friedman, H. L. *Physica* **1964**, *30*, 509; **1964**, *30*, 537.
- (4) Justice, J. C. *J. Phys. Chem.* **1996**, *100*, 1246.
- (5) Born, M. *Z. Physik.* **1920**, *1*, 221.
- (6) Fuoss, R. M. *Proc. Natl. Acad. Sci.* **1959**, *45*, 807.
- (7) Boyd, R. H. *J. Chem. Phys.* **1961**, *35*, 1281.
- (8) Zwanzig, R. *J. Chem. Phys.* **1963**, *38*, 1603; **1970**, *52*, 3625.
- (9) (a) Hubbard, J.; Onsager, L. *J. Chem. Phys.* **1977**, *67*, 4850. (b) Hubbard, J. *J. Chem. Phys.* **1978**, *68*, 1649. (c) Hubbard, J.; Kayser, R. F. *J. Chem. Phys.* **1981**, *74*, 3535; **1982**, *76*, 3377.
- (10) Chen, J. H.; Adelman, S. A. *J. Chem. Phys.* **1980**, *72*, 2819.
- (11) Frank, H. S. in *Chemical Physics of Ionic Solutions*; Conway, Barradas, Eds.; John Wiley & Sons: New York, 1956, p 60.

- (12) (a) Wolynes, P. G. *J. Chem. Phys.* **1978**, *68*, 473. (b) Colonomos, P.; Wolynes, P. G. *J. Chem. Phys.* **1979**, *71*, 2644. (c) Wolynes, P. *Annu. Rev. Phys. Chem.* **1980**, *31*, 345. (d) Hubbard, J.; Wolynes, P. *Theories of Solvated Ion Dynamics*, Chapter 1 In *The Chemical Physics of Ion Solvation*, Part C; Dogonadze, R. R., Kalman, E., Kornyshev, A. A., Ulstrup, J., Eds.; Elsevier: New York, 1985. (e) Hubbard, J. *Non-Equilibrium Theories of Electrolyte Solutions*. In *The Physics and Chemistry of Aqueous Ionic Solutions*; Bellissent-Funel, M. C., Neilson, G. W., Eds.; Reidel Publishing Co.: Dordrecht, 1987.
- (13) (a) Biswas, R.; Roy, S.; Bagchi, B. *Phys. Rev. Lett.* **1995**, *75*, 1098. (b) Biswas, R.; Bagchi, B. *J. Am. Chem. Soc.* **1997**, *119*, 5946–5953. (c) Biswas, R.; Bagchi, B. *J. Chem. Phys.* **1997**, *106*, 5587.
- (14) (a) Lee, S. H.; Rasaiah, J. C. *J. Phys. Chem.* **1996**, *100*, 1420. (b) Lee, S. H.; Rasaiah, J. C. *J. Chem. Phys.* **1994**, *101*, 6964.
- (15) Berendsen, H. J. C.; Grigera, J. R.; Straatsma, T. P. *J. Phys. Chem.* **1987**, *91*, 6269.
- (16) (a) Lynden-Bell, R. M.; Rasaiah, J. C. *J. Chem. Phys.* **1997**, *107*, 1981. (b) Lynden-Bell, R. M.; Rasaiah, J. C. *J. Chem. Phys.* **1996**, *105*, 9266.
- (17) (a) Dang, L. X. *Chem. Phys. Lett.* **1992**, *200*, 21. (b) Dang, L. X.; Garrett, B. C. *J. Chem. Phys.* **1993**, *99*, 2972.
- (18) Smith, D. E.; Dang, L. X. *J. Chem. Phys.* **1994**, *100*, 3757.
- (19) Dang, L. X. *Chem. Phys. Lett.* **1994**, *227*, 211.
- (20) Dang, L. X.; Kollman, P. A. *J. Phys. Chem.* **1995**, *99*, 55.
- (21) Dang, L. X. *J. Am. Chem. Soc.* **1995**, *117*, 6954.
- (22) Dang, L. X. Private communication.
- (23) Dang, L. X. *J. Chem. Phys.* **1992**, *96*, 6970.
- (24) Dang, L. X. *J. Chem. Phys.* **1995**, *102*, 3483.
- (25) Steinhäuser O. *Mol. Phys.* **1982**, *45*, 335; **1982**, *46*, 827.
- (26) Roberts, J. E.; Schnitker, J. *J. Chem. Phys.* **1995**, *99*, 1322.
- (27) Hummer, G.; Pratt, L.; and Garcia, A. E. *J. Phys. Chem.* **1996**, *100*, 1206.
- (28) Jimenez, R.; Fleming, G. R.; Kumar, P. V.; Maroncelli, M. *Nature* **1994**, *369*, 471.
- (29) (a) Jazazeba, A.; Walker, G. C.; Johnson, A. E.; Barbara P. F. *Chem. Phys.* **1991**, *152*, 57. (b) Walker, G.; Akesson, E.; Johnson, A. E.; Levinger, N. E.; Barbara, P. *J. Phys. Chem.* **1992**, *96*, 3728.
- (30) Maroncelli, M.; Fleming, G. *J. Chem. Phys.* **1988**, *89*, 5044; **1990**, *92*, 3151.
- (31) Vijaykumar, P.; Tembe, B. L. *J. Phys. Chem.* **1991**, *95*, 6430.
- (32) Perera, L.; Berkowitz, M. *J. Chem. Phys.* **1992**, *96*, 3092; **1992**, *97*, 5253.
- (33) Neria, E.; Nitzan, A. *J. Chem. Phys.* **1992**, *96*, 5433.
- (34) (a) Fonseca, T.; Ladyani, B. *J. Phys. Chem.* **1991**, *95*, 2116. (b) Fonseca, T.; Ladyani, B. *J. Mol. Liq.* **1994**, *60*, 1.
- (35) Kumar, P. V.; Maroncelli, M. *J. Chem. Phys.* **1995**, *103*, 3038.
- (36) Lin, Y.; Jonah, C. D. *Chem. Phys. Lett.* **1995**, *233*, 138.
- (37) Skaf, M. S.; Ladyani, B. M. *J. Phys. Chem.* **1996**, *100*, 185628.
- (38) Sese, G.; Guardia, E.; Padro, J. A. *J. Chem. Phys.* **1996**, *105*, 8826.
- (39) Stratt, R.; Maroncelli, M. *J. Phys. Chem.* **1996**, *100*, 12981.
- (40) Rips, I.; Klafter, J.; Jortner, J. *J. Chem. Phys.* **1988**, *88*, 3246; *ibid.* **1988**, *89*, 4288.
- (41) Maroncelli, M.; MacInnes, J.; Fleming, G. R. *Science* **1989**, *243*, 1674.
- (42) Bagchi, B. *Annu. Rev. Phys. Chem.* **1989**, *40*, 115 and references therein.
- (43) Fleming, G. R.; Wolynes, P. G. *Phys. Today* **1990**, 36.
- (44) Zhu, J.; Rasaiah, J. C. *J. Chem. Phys.* **1994**, *101*, 9966; **1992**, *96*, 1435; **1991**, *95*, 3325.
- (45) Rasaiah, J. C.; Zhu, J. *J. Chem. Phys.* **1993**, *98*, 1213.
- (46) Gaudel Y.; Rosky, P. J. *Ultrafast Reaction Dynamics and Solvent Effects*; A.I.P. Confer. Proc. Ser. 298; American Institute of Physics: New York, 1994.
- (47) (a) Ranieri, F.; Zhou, Y.; Friedman, H. L. *Chem. Phys.* **1991**, *151*, 201. (b) Friedman, H. L.; Ranieri, F. O.; Hirata, F.; Peng, B. C. *J. Stat. Phys.* **1995**, *78*, 239. (c) Ranieri, F. O.; H. L. Friedman. *J. Chem. Phys.* **1994**, *101*, 6111.
- (48) Impey, R. W.; Madden, P. A.; MacDonald, I. R. *J. Phys. Chem.* **1983**, *87*, 5071.
- (49) Rey, R.; Hynes, J. T. *J. Phys. Condens. Matter.* **1996**, *8*, 9411.
- (50) Rey, R.; Hynes, J. T. *J. Phys. Chem.* **1996**, *100*, 5611.
- (51) Grote, R. F.; Hynes, J. T. *J. Chem. Phys.* **1980**, *74*, 2715.
- (52) Voth, G. *J. Chem. Phys.* **1992**, *97*, 5908.
- (53) Luzar, A.; Chandler, D. *Nature* **1996**, *379*, 55.
- (54) Luzar, A.; Chandler, D. *Phys. Rev. Lett.* **1996**, *76*, 928.
- (55) Carignano, M. A.; Karlstrom G.; Linse, P. *J. Phys. Chem.* **1997**, *101*, 1142.